Presented at 27th Conf. on Weather Analysis and Forecasting/
23rd Conf. on Numerical Weather Prediction,
Chicago, IL, Amer. Met. Soc., July 2015

# 31. AN UPDATED HIGH RESOLUTION HYDROMETEOR ANALYSIS SYSTEM USING RADAR AND OTHER DATA

Keith A. Brewster[1] and Derek R. Stratman[2]
[1]Center for Analysis and Prediction of Storms and [2]School of Meteorology
University of Oklahoma, Norman, OK USA

## 1. INTRODUCTION

For many years the Center for Analysis and Prediction of Storms (CAPS) has been developing and producing real-time high resolution analyses, nowcasts and forecasts. Two major real-time forecasting projects for which CAPS is currently producing forecasts are 1) the Storm Scale Ensemble Forecasts (SSEF) produced for the NOAA Hazardous Weather Testbed (HWT) Spring Experiment (Kong et al., 2015) and 2) real-time analyses and forecasts in support of the Collaborative-Adaptive Sensing of the Atmosphere (CASA) Dallas-Fort Worth (D/FW) Urban Testbed (Philips and Chandrasekar, 2012). In 2015 CAPS produced 3-km grid resolution forecasts over the Continental United States for the HWT on a 5031x3447-km grid. For the D/FW Testbed 400-m grid resolution analyses are generated every 5-min over a 180x180-km domain and 1-km forecasts over a 360x320-km domain are generated whenever rainfall is expected in the testbed. The D/FW Testbed analyses and simulations are done with low latency on modest computing resources. For example, a 2-hr 1-km data analysis, assimilation and forecast is completed about 20 minutes after final data cut-off on couple hundred Xeon cores.

One element of the analyses produced for these systems is the analysis of hydrometeors, including clouds and precipitation-sized rain, snow, ice, and hail and/or graupel. Adjustments to relative humidity and potential temperature are also made with the aim to provide an initial condition that will support the hydrometeors and storm structure and reduce or eliminate the common short-term spin-up required in a number of other mesoscale or storm-scale models initialized without such adjustments.

Recently the hydrometeor analysis has been updated to accommodate new radar data and to customize it for many of the cloud and precipitation microphysics schemes now available in the CAPS Advanced Regional Prediction System (ARPS) and in the Weather Research and Forecasting (WRF) forecast systems.

This work briefly gives an overview of the complex cloud analysis (Section 2) and presents some of the recent changes to the cloud analysis, including those made to the radar pre-processing with quality control and remapping and updates to the hydrometeor assignment algorithms (Section 3). Some examples of its application to 1-km short-term forecasts utilizing the incremental analysis updating (IAU) data assimilation technique over the D/FW Testbed are presented (Section 4) before concluding with a description of some ongoing and future planned work (Section 5).

*Corresponding author address:
Keith Brewster, Ph.D., CAPS/Univ of Oklahoma
120 David Boren Blvd., Suite 2500,
Norman, OK USA 73072 kbrewster@ou.edu

## 2. ADAS Complex Cloud Analysis

The ARPS Data Analysis System (ADAS) Complex Cloud Analysis has its roots in a code from the Local Analysis and Prediction System (LAPS) cloud analysis (Albers et al., 1996), but has evolved and been updated in a number of ways over the years as reported in Zhang et al., 1998, Brewster, 2002, Brewster et al. 2005, and Hu et al. 2006a,b.

In a nutshell, the cloud analysis uses surface and satellite data along with model background data to define the extent and type of cloud. A one-dimensional cloud model considering a parcel lifted from cloud base with entrainment is used to define the quantity of cloud in convective clouds. Radar data is largely used to define the precipitation-sized hydrometeors and to remove spurious precipitation-sized hydrometeors where radar scans are available and no hydrometeor targets were detected. The species type is determined from background temperature, reflectivity, and $Z_{dr}$, or, in the cast of cycling mode, based on the relative distribution of the species in the background forecast.

In prior versions the conversion of radar reflectivity to hydrometeor mass followed three equations, one each for rain, snow and hail. These equations had implicit assumptions about the dropsize distributions of the hydrometeors which were not necessarily consistent with the various microphysics options that are available in ARPS and WRF. For that reason, in this work we seek to customize this conversion; that will be described in Section 3e.

## 3. RECENT UPDATES

The observation processing and analysis code has undergone near-continuous improvement over time to accommodate new data sources, changes to existing data sources and to refine quality control procedures. Notable among the changes made recently are five modifications described here:

### a. NEXRAD Dual-Pol Variables

Changes were made to the radar Cartesian remapping program (*88d2arps*) to read and process the dual-polarization variables now being provided in the Level-II WSR-88D data files. Specifically, the Correlation Coefficient ($\rho_{HV}$), Differential Reflectivity ($Z_{dr}$), and Phase ($\Phi$) variables are now being read from the data files. The correlation coefficient is being used as part of the quality control procedure; a user-specified threshold (default 0.85 for S-Band and 0.75 for X-Band) is applied to help remove non-meteorological targets from the reflectivity and velocity. The $Z_{dr}$ data are remapped to the model Cartesian grid using the same local quadratic fit algorithm that is applied to reflectivity and radial velocity. The remapped $Z_{dr}$ data are then used as part of the algorithm determining hydrometeor type, where grid points with low $Z_{dr}$ and high reflectivity are assigned the hail/graupel type. An algorithm was written to robustly calculate $\Phi_{dp}$ from the $\Phi$ data provided in the WSR-88D data, for future use in estimating rainfall rates and local hydrometeor mixing ratios.

### b. New NEXRAD Volume Coverage Patterns

Recently the Supplemental Adaptive Intra-Volume Low-Level Scan (SAILS) volume coverage pattern (VCP) to the WSR-88D data collection options. In this VCP the antenna returns to lower elevation angles in the middle of the VCP which affected the logic previously applied to determine the end of a volume scan. This logic was modified to avoid the false end-of-volume-scan detection. For SAILS and other VCPs where duplicate sweeps are taken at low elevation angles, the logic was modified to select duplicate sweeps that contain the dual-polarization variables over sweeps that omit the dual-pol data.

### c. New X-band Radar Systems in the CASA D/FW Testbed

The original CASA deployment in Oklahoma consisted of four identical magnetron X-band radars built by the University of Massachusetts (UMass, Mclaughlin et al., 2009). The current CASA D/FW X-band radar network (Figure 1) consists of some of the UMass radars and a variety of radars from three separate manufacturers, including some solid-state radars, such as the Ranger from EEC (Cao et al., 2015). While a network standard has been established for data distribution in single-sweep multi-variable NetCDF files, there remain a number of differences in the data variables and metadata among the files from different providers. The ARPS NetCDF-based radar remapper (*ncrad2arps*) was modified to accommodate these differences and to take advantage of those X-band radars providing signal-to-noise (SNR) measurements in place of a separate algorithm to calculate SNR from reflectivity, range and radar characteristics that is used otherwise. The output remapped data from all radars are presented in a uniform manner to the analysis program.

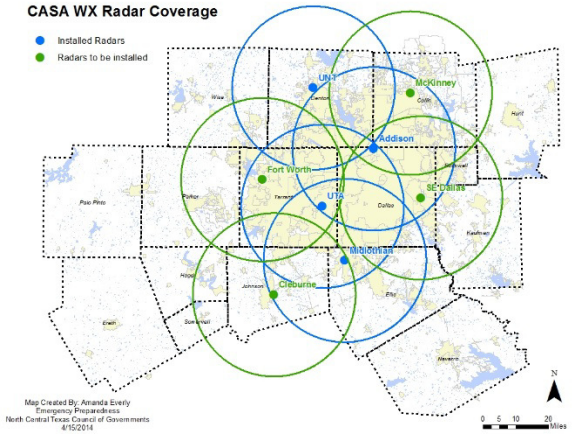


*Fig 1. CASA D/FW Urban Testbed X-band radar network, with each radar indicated by a 40-km range ring, as it existed in early 2015. Subsequently, the radar at Cleburne has been added. With county boundaries of the North Central Texas Council of Governments as dotted lines.*

### d. Removal of hydrometeors below the radar beam

One step of the complex cloud analysis involves removing hydrometeors from the model background field where those variables are provided in the background forecast fields and no meteorological targets are observed according to the quality-filtered, remapped and mosaicked reflectivity. Part of that algorithm involves keeping track of the grid points that have been scanned by the radar(s). Grid points that happen to lie below the radar scanning extent, due to distance from the nearest radar and Earth's curvature, were not modified by the original clearing scheme. This approach was creating hydrometeor analyses with orphaned hydrometeors below the lowest radar scanning elevation when there was a spurious or malpositioned storm that had otherwise been removed aloft.

The updated algorithm keeps track of the extent of hydrometeor removal or reduction in each vertical column. For grid points below 5-km and not observed by radar, the hydrometeor quantities are reduced by the same fraction as the average reduction to the total hydrometeor mass in the grid points above. So, if precipitation is completely removed aloft where the radar observed no echoes, the adjustment ratio is zero, and the hydrometeors are removed from the remaining grid points below the radar coverage extent.

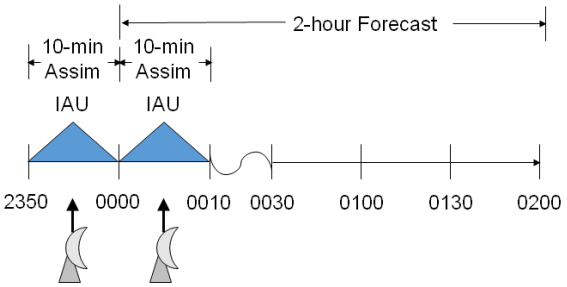


*Figure 2. Timeline for data assimilation strategy in CAPS operational nowcast and short-term forecast in the Dallas/Ft Worth Testbed*

### e. Hydrometeor Retrieval from Reflectivity

As mentioned in Section 2, the original equations for deriving hydrometeor mass from reflectivity were based on a set of equations that did not vary with the microphysics scheme. This created a situation where the reflectivity plotted using the appropriate drop size distribution for the microphysics results would produce an inconsistent output reflectivity. Besides the effect to the graphical output, this inconsistency could affect the forecasts because the microphysics scheme was not getting hydrometeor values consistent with its drop size distribution specifications or assumptions.

To address this issue, the equations for mass-to-radar reflectivity for several of the microphysics schemes supported by the ARPS and WRF models were inverted to create relations for retrieving the hydrometeor mass from the observed reflectivity. The schemes that were addressed include the Lin 5-class Ice microphysics scheme (Lin et al, 1983), the WRF single-moment 6-class (WSM6, Hong and Lin, 2006) microphysics scheme, Thompson scheme (Thompson et al., 2008), Milbrandt and Yau (MY) single-moment bulk microphysics scheme, MY double-moment bulk microphysics scheme, and MY triple-moment bulk microphysics scheme (Milbrandt and Yau, 2005a,b). Equations and constants provided in the WRFpost and ARPSplt programs are used as the basis for the retrieval code.

In some cases the equations did not have a unique inversion because the hydrometeor mass was involved in determining a drop size distribution shape parameter. In those cases the background or a seed value for the hydrometeor mass was first provided to find an initial value for the shape parameter and a solution was found iteratively. After testing each scheme in a standalone program it was found that convergence is obtained quickly, so five iterations are done in those cases.

## 4. Demonstration of Updated System

In order to demonstrate the latest version of the cloud analysis and the morphology of the hydrometeors in the model during the incremental analysis period a case of a mature squall line with hail over the Dallas-Fort Worth metroplex is chosen. We chose the case of 0000 UTC 25 April for this demonstration. This is a challenging case for the modeling system as strong updrafts associated with the hail will have to be established and the large mass of hydrometeors supported. The ARPS model will be used with cycled incremental analysis updating (IAU) applied as indicated in Fig 2. Data from 2350-0000 UTC are used to form an analysis and analysis increments to apply during that 10-minute window. A triangular time weighting is used to introduce the increments. Then, in the same manner, data from 0000-0010 are introduced in the next cycle.

First we examine the impact of the revised reflectivity equations on the plotted reflectivity. Figure 3 shows the observed mosaicked reflectivity in a horizontal (model level 8) and vertical cross section (y=40.5 km) at the top. In the left column is the output reflectivity using the reflectivity forward model from four different microphysics schemes. In the center column is the same horizontal cross-section after applying the microphysics-scheme-specific hydrometeor retrieval algorithms. It is evident that the original scheme introduced inconsistencies that varied from under-representing the maximum in the case of the Lin scheme, to overstating the maximum in the MY schemes. Note that grid points with reflectivity less than a user-defined threshold (15 dBZ at this level) are not assigned hydrometeors to help prevent residual non-meteorological targets from being used near the ground. The vertical cross-section plots (right hand column) confirm that the hydrometeor mass scheme has recovered values consistent with each method's forward model for reflectivity for all heights/temperatures.

Figure 4 shows a sample vertical cross-section (at Y=40.5 km) of the hydrometeors retrieved for each scheme. There is little difference among the rain mass values (left column) whereas there are more significant differences among the frozen hydrometeors, particularly graupel (center) and hail (color shading in right column).

Having confirmed successful retrieval of the hydrometeor mass in the analysis it is of interest to see how well the model adapts to these increments being applied during the IAU window. Figure 5 shows the same sample cross-section after the increments from the analysis are applied over a 10-minute IAU window, which can be compared to the original, input, analysis or the second analysis (Fig 6) valid 10-minutes later. It is apparent that all schemes have some difficulty in maintaining the maximum values of hail and/or graupel, with the WSM-6 retaining the highest value of graupel. The Lin and WSM-6 schemes end-up with greater rain water than the analyses possibly due to the hail or graupel falling and melting. The MY-Double Moment

scheme seems to have retained the best structure in this sample vertical cross-section after the first cycle.

As indicated the operational forecasts have a second cycle. During this cycle the background ratios between the hydrometeor species (in reflectivity, Z, space) are preserved, and then the total quantities are updated to match the observed total reflectivity, again using the customized reflectivity retrieval equations. Also in this pass latent heat and water vapor are not added, to avoid pumping too much heat and water into the system.

The results after the second IAU wind are shown in Fig. 8. As in the first cycle, some excess rain is observed in the Lin and WSM-6 schemes, and in this cycle the cores advance to the east beyond the analysis extent. After the second IAU window there is a general increase in the hail and graupel aloft, which is likely due to the updraft having accelerated to sufficient speed to loft frozen hydrometeors higher by this time.

## 5. Conclusions and Future Plans

A number of updates have been applied to the hydrometeor retrieval in the ADAS Complex Cloud Analysis and these will be applied to the ongoing forecasting efforts at CAPS.

In a related study many of these updates were applied to a case study involving multiple interacting supercell storms on 24 May 2011 (Stratman and Brewster, 2015). The simulations using the 3DVAR and cloud analysis a single-cycle IAU system, produced some notable successes in predicting these storms, including some remarkably accurate predictions of rotation centers in the storms.

Examining the vertical cross sections in this way underscored the difficulties in establishing an updraft in a strong convective storm from a larger-scale background without such a storm. There was some evidence in the first cycle of difficulty in maintaining the observed hail/graupel maxima. In this demonstration, as in our current real-time system, the increments from all variables are applied using same triangular distribution with the largest increments applied in the middle of the time window (as indicated in Fig 2.). It may be possible to improve the support of the weight of the hail and heavy rain by applying more of the latent heat increments before the hydrometeors to allow the updraft velocities to become established without rain and hail loading, and possible decelerating cooling due to ice melt. This can be accomplished by adjusting the increment distribution in time so that a larger fraction of the latent heat increments are applied early in the IAU window while the hydrometeors are introduced using a different time weighting that applies most of those increments toward the end of the IAU window (Fig 8). The capability for this will be added to the software and tested in the near future.

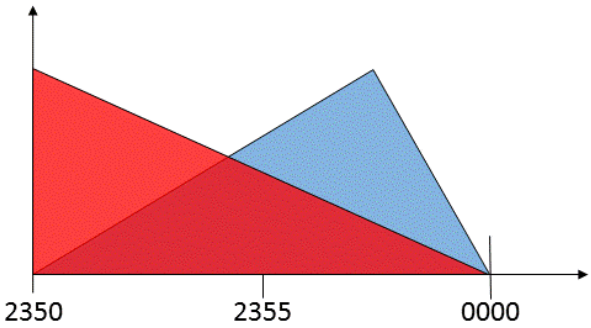


*Fig 8. Proposed IAU increment distribution scheme, showing distribution of increments for potential temperature and wind (red) leading the distribution of other variables, including hydrometeors (blue).*

## 6. Acknowlegments

The D/FW Urban Testbed and CASA work are supported in part by the National Science Foundation (NSF) under EEC03-13747, by the NWS Network of Networks National Mesonet Project, the NCTCOG, and other local government and private sector partners. Analysis development and testing for real-time modeling at CAPS is also supported by the NOAA Warn-on-Forecast project, Chinese Meteorological Agency, Jiangsu Province and Shenzhen City forecast projects. OU OSCER (Boomer) supercomputing resources were used in this study and in our real-time forecast efforts. Any opinions, findings, conclusions, or recommendations expressed in this material are those of the authors and do not necessarily reflect those of the funding agencies.

## 7. References

Albers, S. C., J. A. McGinley, D. A. Birkenheuer, and J. R. Smart, 1996: The Local Analysis and Prediction System (LAPS): Analysis of Clouds, Precipitation and Temperature. *Wea. Forecasting*, **11**, 273–287.

Bloom, S. C., L. L. Takacs, A. M. da Silva, and D. Ledvina, 1996: Data Assimilation Using Incremental Analysis Updates. *Mon. Wea. Rev.*, 124, 1256–1271.

Brewster, K., 2002: Recent advances in the diabatic initialization of a non-hydrostatic numerical model. *Preprints, 21st Conf. on Severe Local Storms*, and *Preprints, 15th Conf. Num. Wea. Pred. and 19th Conf. Wea. Anal. Forecasting*, San Antonio, TX, Amer. Meteor. Soc., J51-54.

Brewster, K., M. Hu, M. Xue, and J. Gao, 2005: Efficient assimilation of radar data at high resolution for short range numerical weather prediction. World Weather Research Program Symposium and

Nowcasting and Very Short-Range Forecasting WSN05, Toulouse, France. WMO World Weather Research Program, Geneva, Switzerland. Symposium CD, Paper 3.06.

Cao, Q.; Knight, M.; Helvin, J.; Stafford, R.; Free, A., 2015: "EEC's next generation weather radar: Solid-state polarimetric weather radar with advanced time-frequency multiplexing waveform design," Radar Conference (RadarCon), 2015 IEEE , vol., no., pp.0723,0727, , doi:10.1109/RADAR.2015.7131091

Gao, J., M. Xue, K. Brewster, and K. K. Droegemeier, 2004: A three-dimensional variational data analysis method with recursive filter for Doppler radars. *J. Atmos. Oceanic Tech.*, 21, 457-469.

Hong, S.-Y., and J.-O. J. Lim, 2006: The WRF single-moment 6-class microphysics scheme (WSM6). *J. Korean Meteor. Soc.*, 42, 129–151.

Hu, M., M. Xue, and K. Brewster, 2006: 3DVAR and Cloud Analysis with WSR-88D Level-II Data for the Prediction of the Fort Worth, Texas, Tornadic Thunderstorms. Part I: Cloud Analysis and Its Impact. *Mon. Wea. Rev.*, 134, 675–698.

Hu, M., M. Xue, J. Gao, and K. Brewster, 2006: 3DVAR and Cloud Analysis with WSR-88D Level-II Data for the Prediction of the Fort Worth, Texas, Tornadic Thunderstorms. Part II: Impact of Radial Velocity Analysis via 3DVAR. *Mon. Wea. Rev.*, 134, 699–721.

Kong, F., M. Xue, Y. Jung, K.A. Brewster, K.W. Thomas, Y. Wang, F. Shen, I.L. Jirak, A. Clark, J. Correia, Jr., S.J. Weiss, M.C. Coniglio, C.J. Melick, 2015: An Overview of CAPS Storm-Scale Ensemble Forecast for the 2015 HWT Spring Forecasting Experiment. *Preprints, 27th Conf. on WAF and 23rd Conf. on NWP*, Chicago, IL, Amer. Met. Soc., Paper 32.

Lin, Y.-L., R. D. Farley, and H. D. Orville, 1983: Bulk Parameterization of the Snow Field in a Cloud Model. *J. Climate Appl. Meteor.*, 22, 1065–1092.

McLaughlin, D., D. Pepyne, B. Philips, J. Kurose, M. Zink, E. Knapp, D. Westbrook, E. Lyons, A. Hopf, A. DeFonzo, R. Contreras, T. Djaferis, E. Insanic, S. Frasier, V. Chandrasekar, F. Junyent, N. Bharadwaj, Y. Liu, and Y. Wang, K. Droegemeier, M. Xue, J. Brotzge, F. Carr, K. Kloesel, K. Brewster, S. Cruz-Pol, and K. Hondl, 2009: Short-Wavelength Technology and the Potential for Distributed Networks of Small Radar Systems, *Bull. Amer. Meteor. Soc.*, 90, 1797-1817.

Milbrandt, J. A. and M. K. Yau, 2005a: A Multimoment Bulk Microphysics Parameterization. Part I: Analysis of the Role of the Spectral Shape Parameter. *J. Atmos. Sci.*, 62, 3051–3064.

Milbrandt, J. A. and M. K. Yau, 2005b: A Multimoment Bulk Microphysics Parameterization. Part II: A Proposed Three-Moment Closure and Scheme Description. *J. Atmos. Sci.*, 62, 3065–3081.

Philips B., V. Chandrasekar, 2012: "The Dallas Fort Worth urban remote sensing network." IEEE IGARSS 2012: 6911-6913.

Schenkman A. D., M. Xue, A. Shapiro, K. Brewster, and J. Gao, 2011: Impact of CASA Radar and Oklahoma Mesonet Data Assimilation on the Analysis and Prediction of Tornadic Mesovortices in an MCS. *Mon. Wea. Rev.*, 139, 3422–3445.

Stensrud, D. J., L. J. Wicker, K. E. Kelleher, M. Xue, M. P. Foster, J. T. Schaefer, R. S. Schneider, S. G. Benjamin, S. S. Weygandt, J. T. Ferree, and J. P. Tuell, 2009: Convective-Scale Warn-on-Forecast System. *Bull. Amer. Meteor. Soc.*, 90, 1487–1499.

Stensrud, D. J., L. J. Wicker, M. Xue, D. T. Dawson, N. Yussouf, D. M. Wheatley, T. E. Thompson, N. A. Snook, T. M. Smith, A. D. Schenkman, C. K. Potvin, E. R. Mansell, T. Lei, K. M. Kuhlman, Y. Jung, T. A. Jones, J. Gao, M. C. Coniglio, H. E. Brooks, K. A. Brewster, 2013: Progress and challenges with Warn-on-Forecast. *Atmos. Res.*, 123, 2-16.

Stratman, D.R. and K.A. Brewster, 2015: Verification of 24 May 2011 Simulated Mesocyclones Using Variaous Microphysics Schemes at 1-km Grid Resolution. *Preprints, 27th Conf. on WAF and 23rd Conf. on NWP*, Chicago, IL, 2 July 2015.

Thompson, Gregory, Paul R. Field, Roy M. Rasmussen, William D. Hall, 2008: Explicit Forecasts of Winter Precipitation Using an Improved Bulk Microphysics Scheme. Part II: Implementation of a New Snow Parameterization. *Mon. Wea. Rev.*, **136**, 5095–5115.

Xue, M., K. K. Droegemeier, and V. Wong, 2000: The Advanced Regional Prediction System (ARPS) - A multiscale nonhydrostatic atmospheric simulation and prediction tool. Part I: Model dynamics and verification. *Meteor. Atmos. Physics.*, 75, 161-193.

Xue, M., K. K. Droegemeier, V. Wong, A. Shapiro, K. Brewster, F. Carr, D. Weber, Y. Liu, and D.-H. Wang, 2001: The Advanced Regional Prediction System (ARPS) - A multiscale nonhydrostatic atmospheric simulation and prediction tool. Part II: Model physics and applications. *Meteor. Atmos. Physics.*, 76, 134-165.

Xue, M., D.-H. Wang, J.-D. Gao, K. Brewster, and K. K. Droegemeier, 2003: The Advanced Regional Prediction System (ARPS), storm-scale numerical weather prediction and data assimilation. *Meteor. Atmos. Physics*, 82, 139-170.

Zhang, J., F. Carr and K. Brewster, 1998: ADAS cloud analysis. *Preprints, 12th Conf. on Num. Wea. Prediction.*, Phoenix, AZ, Amer. Meteor. Soc., Boston, 185-188.

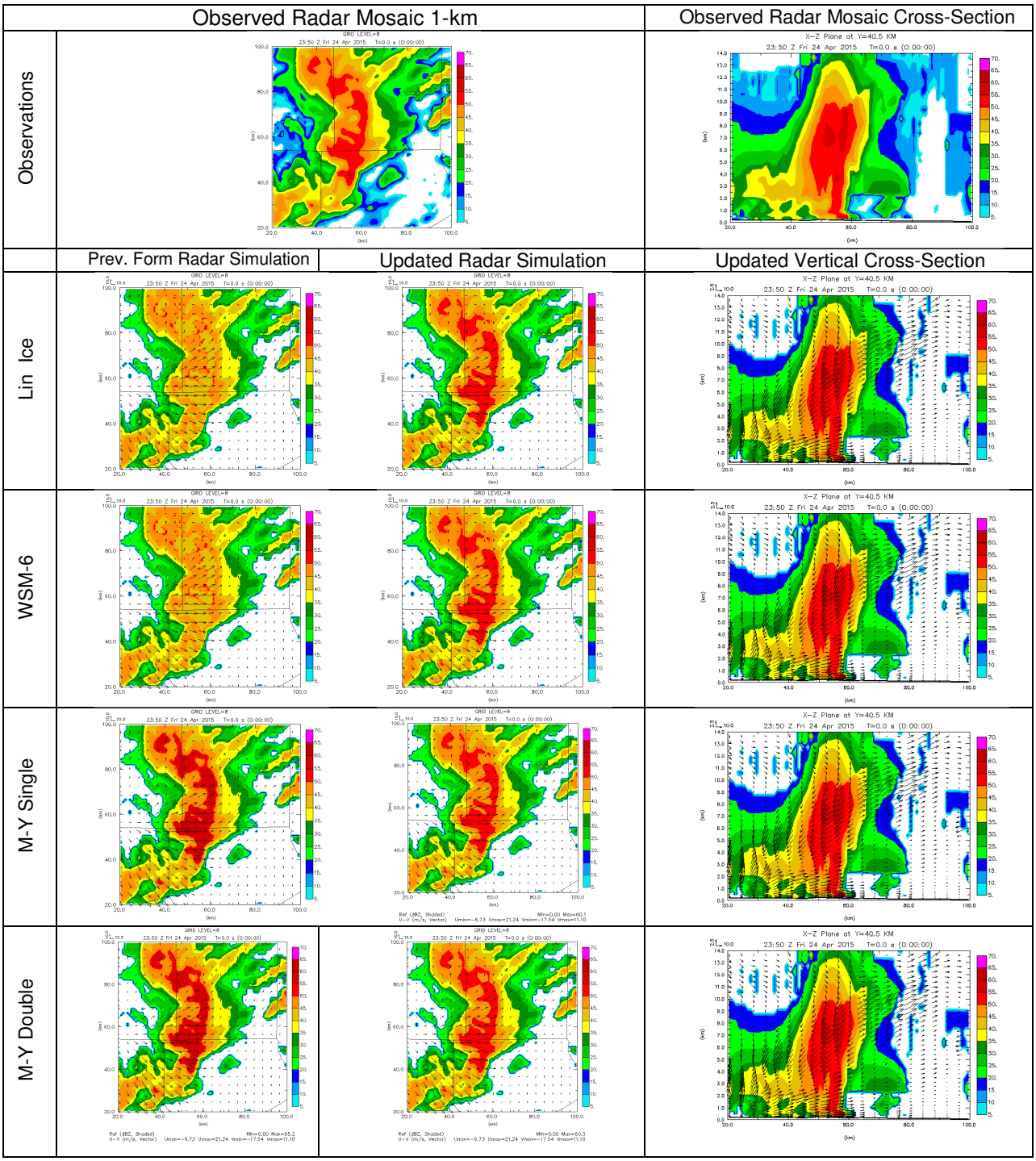


*Figure 3. Validation of radar reflectivity inversion for four different microphysics schemes. Top row: Lin Ice; 2nd row: WSM-6, 3rd M-Y Single Moment, 4th row: M-Y Double moment. First column, radar reflectivity produced after using original radar reflectivity inversion equations for all microphysics schemes. Second column, after using custom inversion scheme for each microphysics scheme. Third column: vertical cross section using custom inversion.*

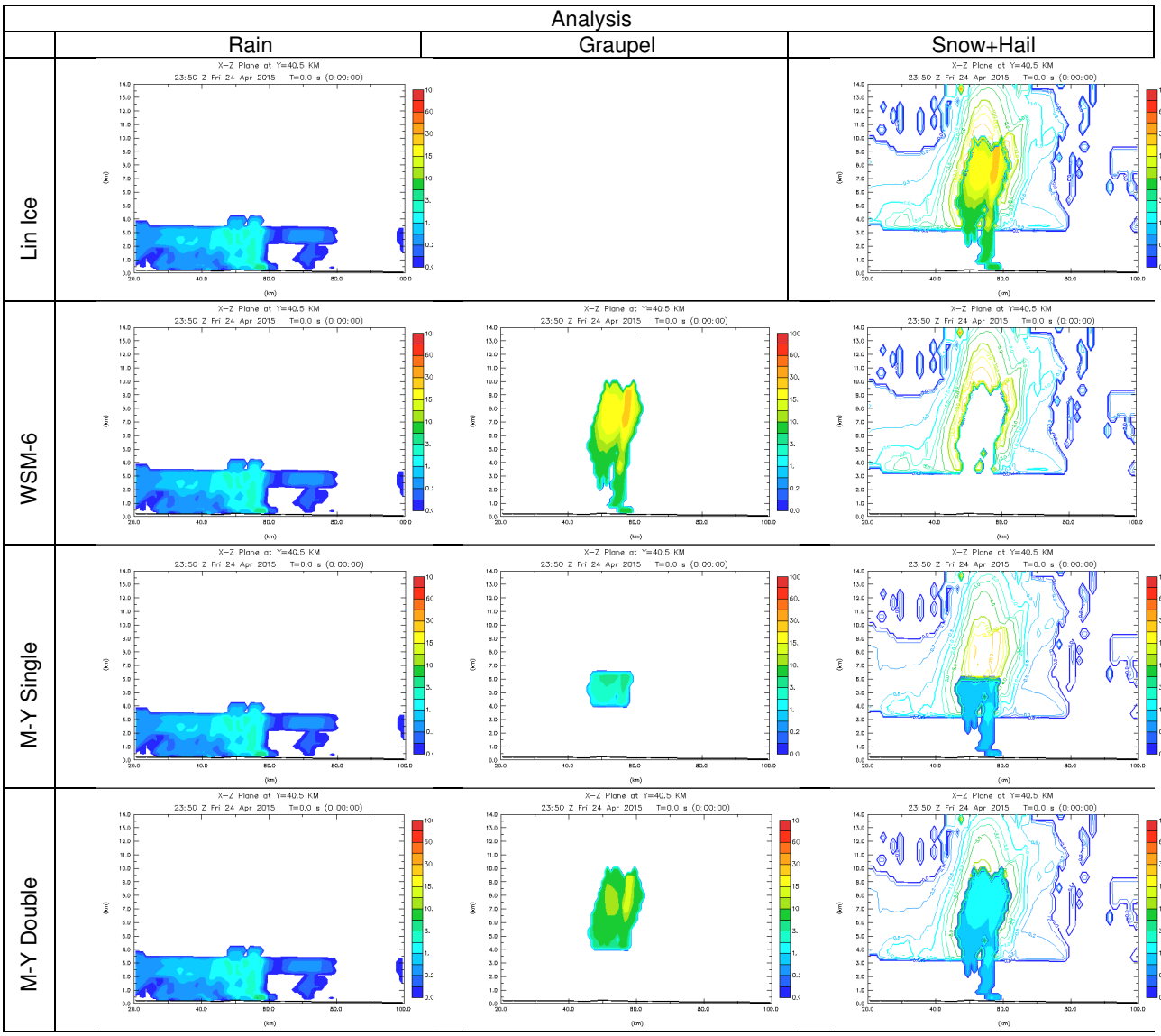


*Figure 4. Analyses of hydrometeors for at 25 April 2015 0000 UTC for four different microphysics schemes. Top row: Lin Ice; 2nd row: WSM-6, 3rd M-Y Single Moment, 4th row: M-Y Double moment. For four types of hydrometeors, First column: rain (g kg$^{-1}$), 2nd: graupel (g kg$^{-1}$), 3rd hail (g kg$^{-1}$, color fill) and snow (g kg$^{-1}$, contours). Contours are color-coded for quantitative value.*

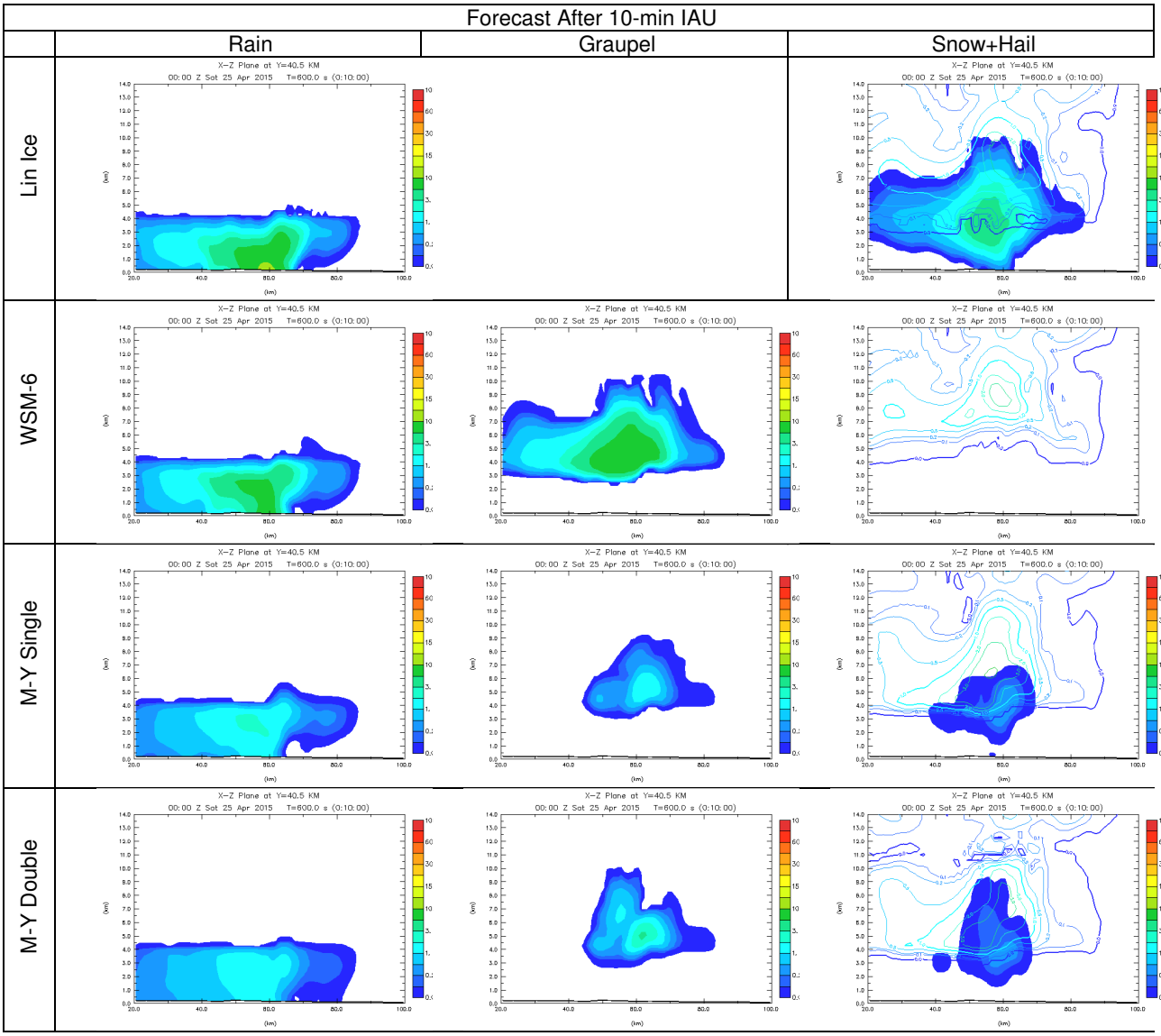


Figure 5. As in Fig. 4, but after 10 minutes of Incremental Analysis Updating beginning at 2350 UTC and ending at 0000 UTC, 25 April 2015.

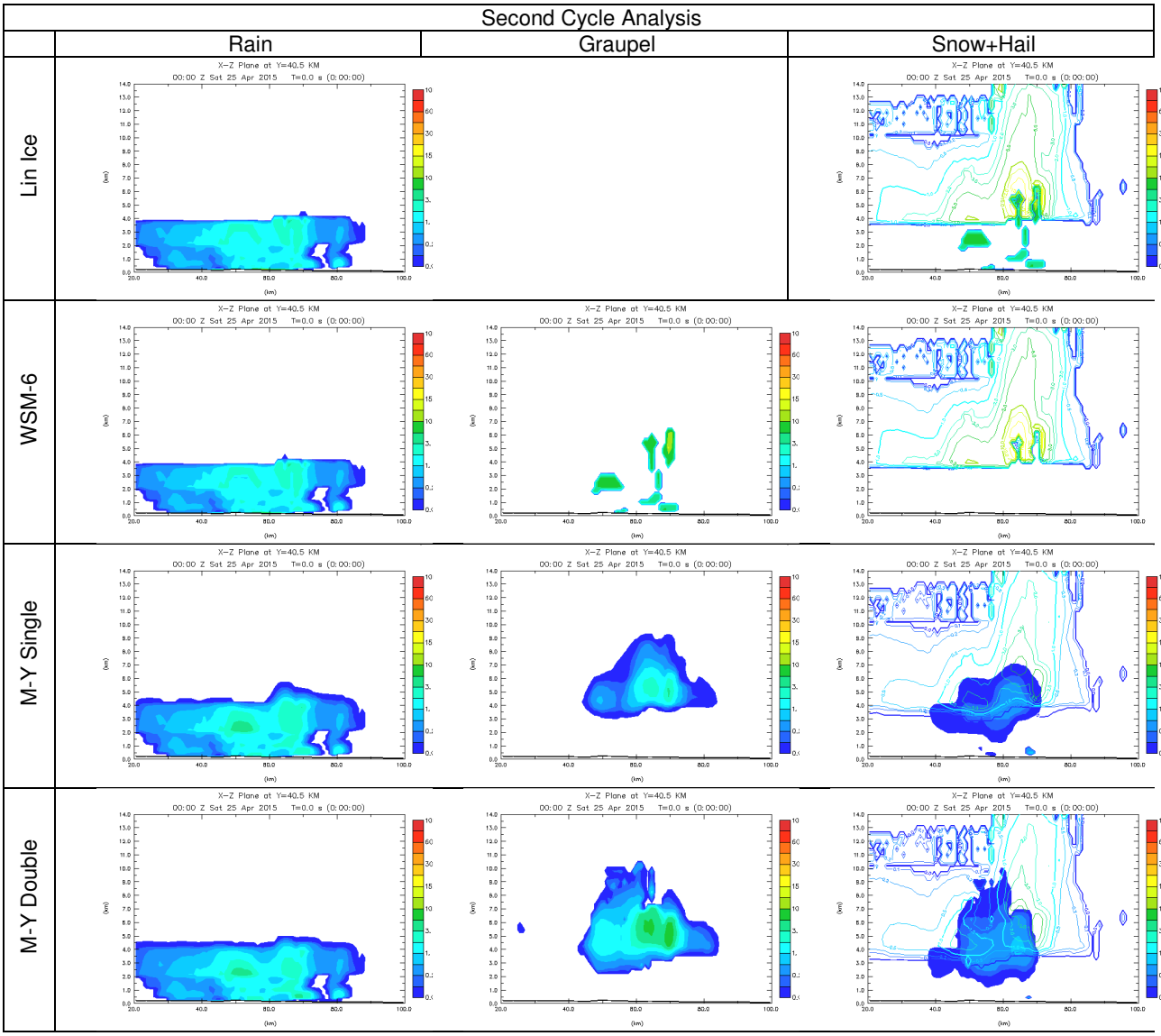


Figure 6. As in Fig. 4, but analysis using radar data valid between 0000 and 0010 UTC 25 April 2015.

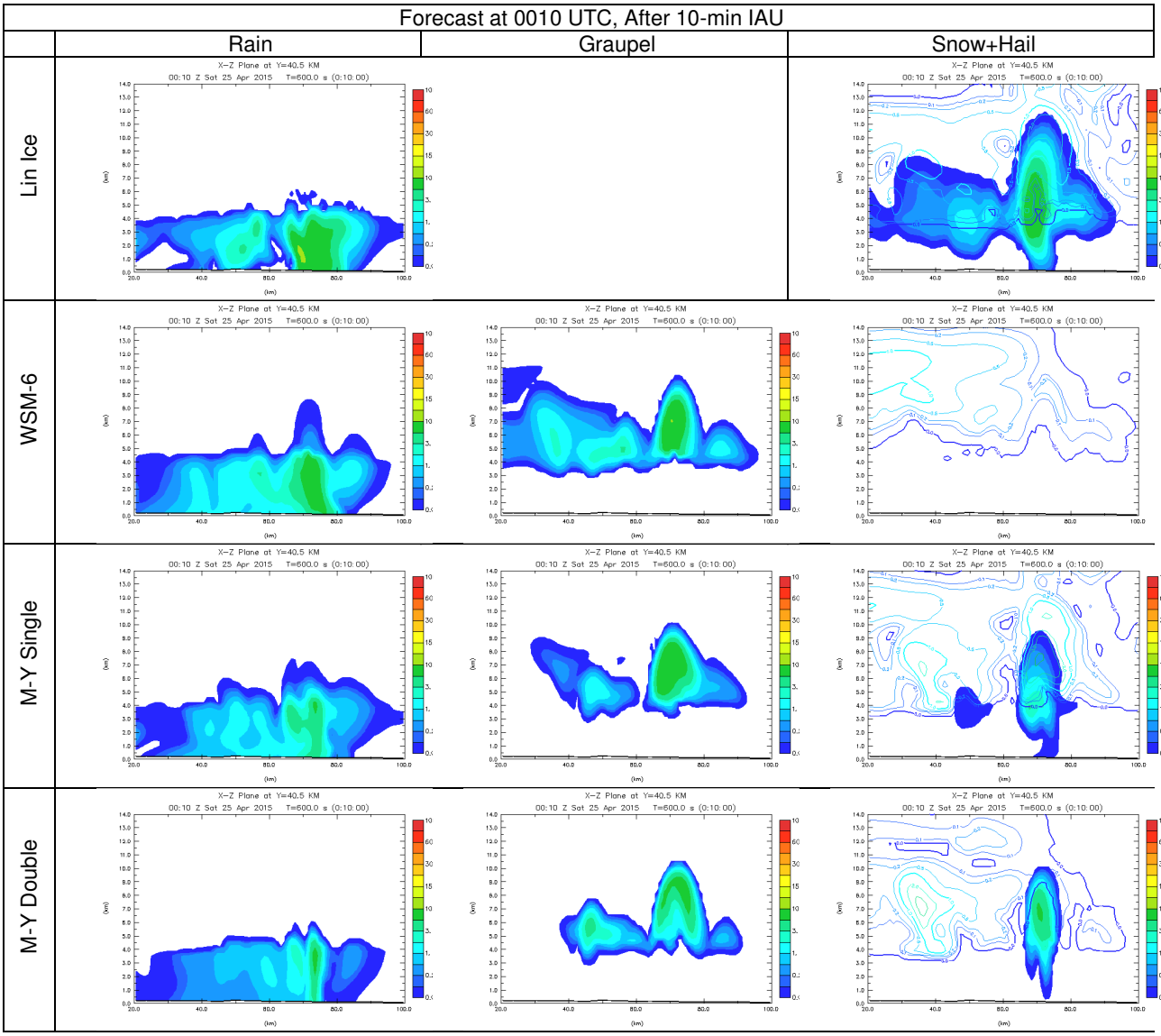


Figure 7. As in Figure 4, but after 10 minutes of Incremental Analysis Updating beginning at 0000 UTC and ending at 0010 UTC, 25 April 2015.